that of ultrasound B-mode imaging, with the exception that OCT uses light instead of sound. OCT has been clinically applied in the field of ophthalmology for the imaging of the retina and cornea (8,9), as well as in dermatology (10,11). The clinical use of this imaging method has also been extended to the field of cardiology for intravascular imaging of the coronary vessels (12). OCT imaging of the inner ear of normal extracted cochlea (13) and the inner ear structure of living rodents has been reported (14,15). OCT was also used to visualize the pathologic morphology of the tectorial membrane in the isolated cochlea of transgenic Tecta mice, with the apical bony wall removed (16).

The aim of this study was to examine the potential of OCT for the analysis of cochlear pathogenesis in living animals with the bony capsule intact. *Slc26a4* knockout mice are well known as a model for Pendred syndrome (17). In this study, we tested the efficacy of OCT for the visualization of endolymphatic hydrops in living *Slc26a4*$^{(-/-)}$ mice.

MATERIALS AND METHODS

Animals

Mice with targeted disruption of *Slc26a4* (17) and their littermates (*Slc26a4*$^{(-/-)}$, *Slc26a4*$^{(+/-)}$, and *Slc26a4*$^{(+/+)}$) at the age of 11 weeks after birth were used in this study. Animals were maintained at the Institute of Laboratory Animals, Kyoto University, Japan. The Animal Research Committee of the Graduate School of Medicine, Kyoto University, approved all experimental protocols, which were performed in accordance with the National Institute of Health Guidelines for the Care and Use of Laboratory Animals (Approval numbers: MedKyo11516 and MedKyo12172. Primary investigator: TS).

Auditory Function

Auditory brainstem responses (ABRs) were recorded to assess the auditory functions of the experimental animals, as previously described (18). The PowerLab/4sp data acquisition system (AD Instruments, Castle Hiss, Australia) was used for the generation of acoustic stimuli and subsequent recording of the evoked potentials. After the mice had been placed under general anesthesia, subdermal stainless steel needle electrodes were inserted at the vertex (ground), ventrolateral to the measured ear (active), and contralateral to the measuring ear (reference). The acoustic stimuli, consisting of tone burst stimuli (cos^2 rise/fall with a 0.1-ms gate time and a 10-ms plateau) were delivered monoaurally through a speaker (ES1spc; Bioresearch Center, Nagoya, Japan) with a funnel that was fitted into the external auditory meatus. The responses between the ground and the active electrodes were amplified with a digital amplifier (MA2, Tucker-Davis Technologies, Alachua, FL, USA). ABR recordings were performed at frequencies of 8, 16, and 32 kHz.

Optical Coherence Tomography

OCT images in living mice (*Slc26a4*$^{(-/-)}$, *Slc26a4*$^{(+/-)}$, and *Slc26a4*$^{(+/+)}$; n = 2 for each class) were obtained using the OCS1300SS OCT system (Thorlabs, New Jersey, USA), which was equipped with a swept-source light source with a central wavelength of 1,300 nm, a spectral bandwidth of 100 nm, and an average output power of 10 mW. The axial scan rate was 16 kHz. The theoretical axial resolution in water is 9 μm. After the mice were placed under general anesthesia with an intraperitoneal injection of medetomidine (0.5 mg/kg), midazolam (13.3 mg/kg), and butorphanol (0.6 mg/kg), the bulla of the left ear was removed to expose the cochlea. Next, the animal was placed on the scanning stage of the OCT system so that the scanning plane (X-Z plane) was parallel to the midmodiolar section (Fig. 1). OCT images were then obtained.

Histologic Assessment

Immediately after the OCT image acquisition, the animals were euthanized with carbon dioxide and then intracardially perfused with 0.01 M phosphate buffered saline (PBS) at pH 7.4, followed by 4% paraformaldehyde (PFA) in 0.01 M PBS at pH 7.4. Next, the temporal bones were excised, perilymphatically perfused with 4% PFA, and immersed in 4% PFA at 4°C for 4 hours. The specimens were then decalcified with 10% ethylenediamine tetraacetic acid for 7 days. The samples were subsequently embedded and frozen in Tissue-Tec OCT compound (Sakura Finetek, Japan), and midmodiolar cryosections were obtained at a thickness of 10 μm. The cryosections were then stained with hematoxylin and eosin (HE) and viewed with an optical microscope (DP70, Olympus, Japan).

For more detailed morphologic comparisons, cochleae from equivalent mice (*Slc26a4*$^{(+/+)}$, *Slc26a4*$^{(+/-)}$, and *Slc26a4*$^{(-/-)}$) were

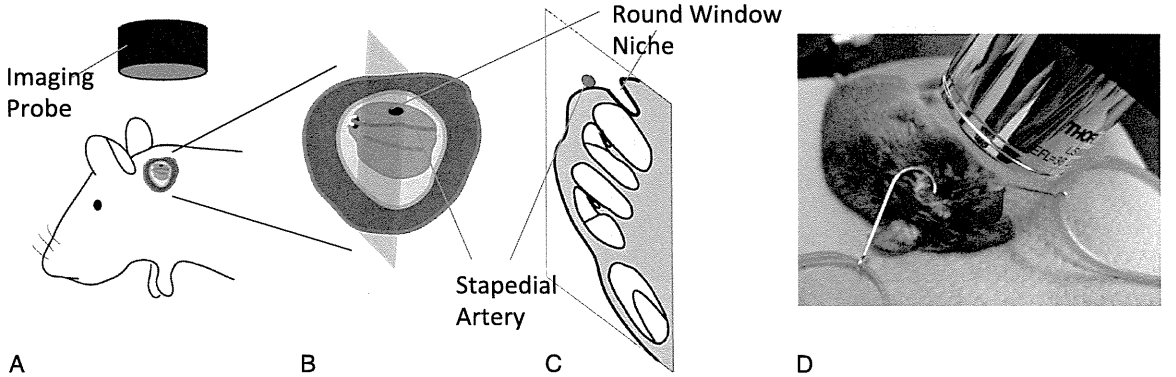

FIG. 1. The scheme of the OCT imaging procedure after surgery. *A*, The mouse was placed under the OCT imaging probe after the exposure of the cochlea. *B*, An enlargement of the surgical field. The optimal section is shown by the rectangle parallel to the modiolus. *C*, The cross section of the intracochlear structures represented by the *rectangle* shown in (*B*). *D*, An overview of the objective lens (outer diameter is 34 mm, working distance is ~25 mm). The animal has been placed on the imaging stage.

isolated, fixed, paraffin-embedded, sectioned at a thickness of 10 μm, stained with HE, and viewed with the optical microscope.

Repeated Observation of the Cochlea Using OCT

For the repeated observation of the cochlea, *Slc26a4*$^{(+/+)}$ mice were used (n = 4). After the first visualization using OCT, the retroauricular skin incision was closed by a nylon monofilament suture, and the animals were maintained in heat-controlled cages. Antibiotic was not administrated. Three or 7 days later, each animal was anesthetized, and OCT images were obtained. The mice were then sacrificed for cryosections as above.

RESULTS

Auditory Functions

The mean left hearing thresholds at the frequencies of 8, 16, and 32 kHz were 10, 15, and 57.5 dB in the *Slc26a4*$^{(+/+)}$ mice and 10, 5, and 30 dB in the *Slc26a4*$^{(+/-)}$ mice,

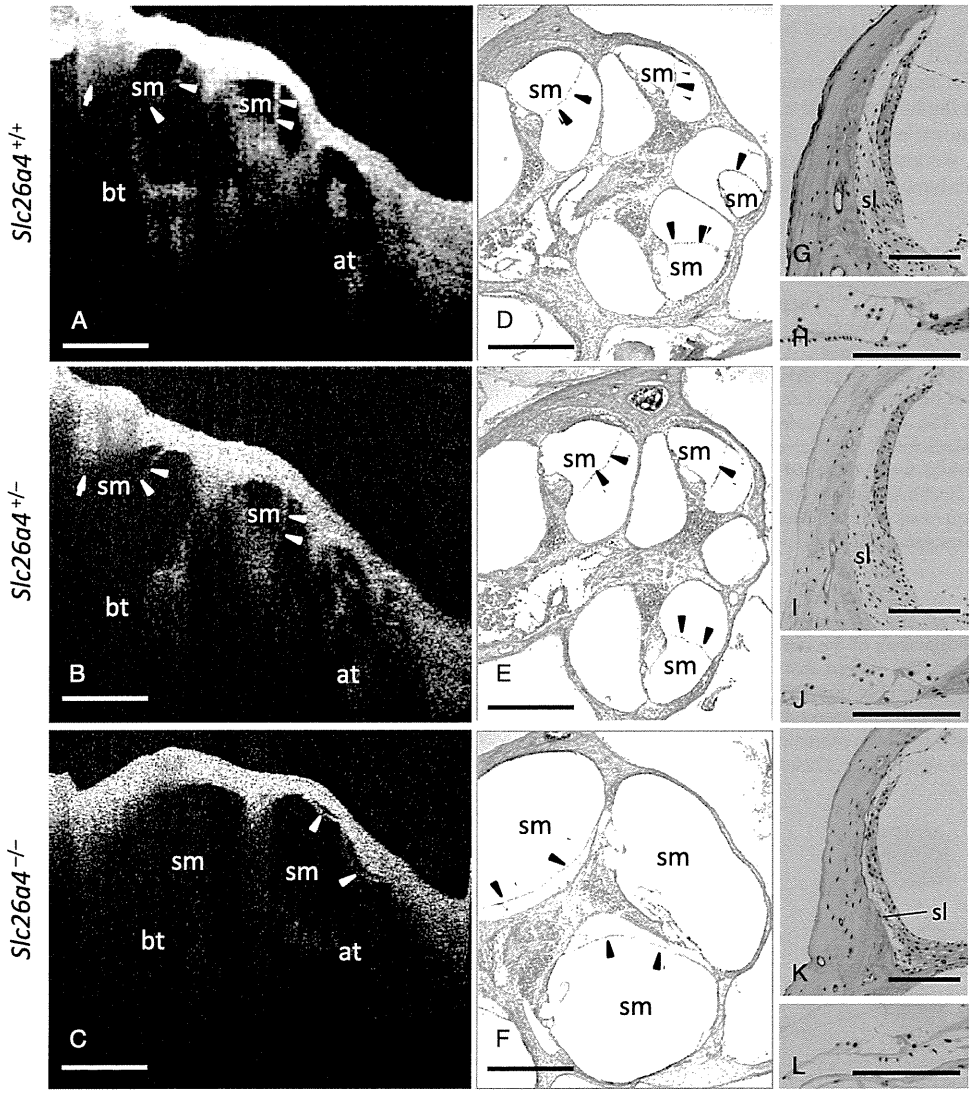

FIG. 2. OCT images and HE staining. *A*, OCT images from a *Slc26a4*$^{(+/+)}$ mouse 11 weeks after birth: apical turn, **at;** basal turn, **bt**; scala media, **sm**. The *arrowheads* indicate the position of Reissner's membrane, and the *arrow* shows the stapedial artery. Reissner's membrane was visualized as a straight, relatively thin structure. *B*, OCT images from a *Slc26a4*$^{(+/-)}$ mouse 11 weeks after birth. The findings were similar to those of a *Slc26a4*$^{(+/+)}$ mouse. *C*, OCT images from a *Slc26a4*$^{(-/-)}$ mouse 11 weeks after birth. Reissner's membrane was positioned close to the bony wall of the scala vestibuli, indicating severe dilatation of the scala media. The cochlea had one and a half turns. *D*, HE staining of the mouse as shown in (*A*). *E*, HE staining of the mouse as shown in (*B*). *F*, HE staining of the mouse as shown in (*C*). (*G, H*), HE staining of a *Slc26a4*$^{(+/+)}$ mouse 11 weeks after birth: spiral ligament, **sl**. (*I* and *J*), HE staining of a *Slc26a4*$^{(+/-)}$ mouse. (*K* and *L*), HE staining of a *Slc26a4*$^{(-/-)}$ mouse. (*A–F*), Scale bars = 500 μm, (*G–L*), Scale bars = 100 μm.

respectively. In the *Slc26a4*$^{(-/-)}$ mice, no ABR waves were detected at the maximum sound intensities, similar to previous findings (17).

OCT Images

Reissner's membrane in the basal and second turns was clearly demonstrated in the *Slc26a4*$^{(+/+)}$ mice (Fig. 2A) and was visualized as straight lines dividing the scala vestibuli and the scala media. The basilar membrane in the second turn was also depicted. Therefore, the area of the scala media of the second turn was clearly identified by visualization of Reissner's membrane, the lateral bony wall, the basilar membrane, and the cochlear spiral limbus. The cochlear modiolus was detected only at the peripheral end between the apical and second turns. The absorption of light by hemoglobin in the stapedial artery caused the visualization of the area below the vessel to be difficult, concealing the basilar membrane of the basal turn and the vestibule. We therefore chose the second turn for the estimation of endolymphatic hydrops. In the apical turn, the helicotrema was illustrated.

Slc26a4$^{(+/-)}$ mice exhibited similar OCT images to those in *Slc26a4*$^{(+/+)}$ mice (Fig. 2B). The scala media in the second turn showed no dilatation, as demonstrated by straight Reissner's membrane of the second turn, as well by the other surrounding structures, including the basilar membrane, the lateral bony wall, and the cochlear spiral limbus.

The cochlea of *Slc26a4*$^{(-/-)}$ mice had one and a half turns, as previously described (17) (Fig. 2C). In the apical turn, Reissner's membrane was found close to the bony wall of the scala vestibuli, indicating severe dilatation of the scala media. Moreover, the basilar membrane in the apical turn was invisible, suggesting it was appressed to the bony wall of the scala tympani. The size of each turn in the *Slc26a4*$^{(-/-)}$ mice was relatively greater compared with those of *Slc26a4*$^{(+/+)}$ and *Slc26a4*$^{(+/-)}$ mice. The modiolus and the cochlear spiral limbus were not visualized.

HE Staining

In *Slc26a4* $^{(+/+)}$ and *Slc26a4* $^{(+/-)}$ mice, the normal coiling of the 2 and a half turns was confirmed (Fig. 2, D and E). As visualized in the OCT cross sections, Reissner's membrane was found to be straight without convexity, and the scala media was not dilated. The organ of Corti (Fig. 2, H and J), the spiral ligament (Fig. 2, G and H), the spiral ganglions, and the modiolus had no degeneration.

In *Slc26a4* $^{(-/-)}$ mice, the decreased number of turns was histologically confirmed (Fig. 2F). Reissner's membrane showed marked convexity and was close to the bony wall of

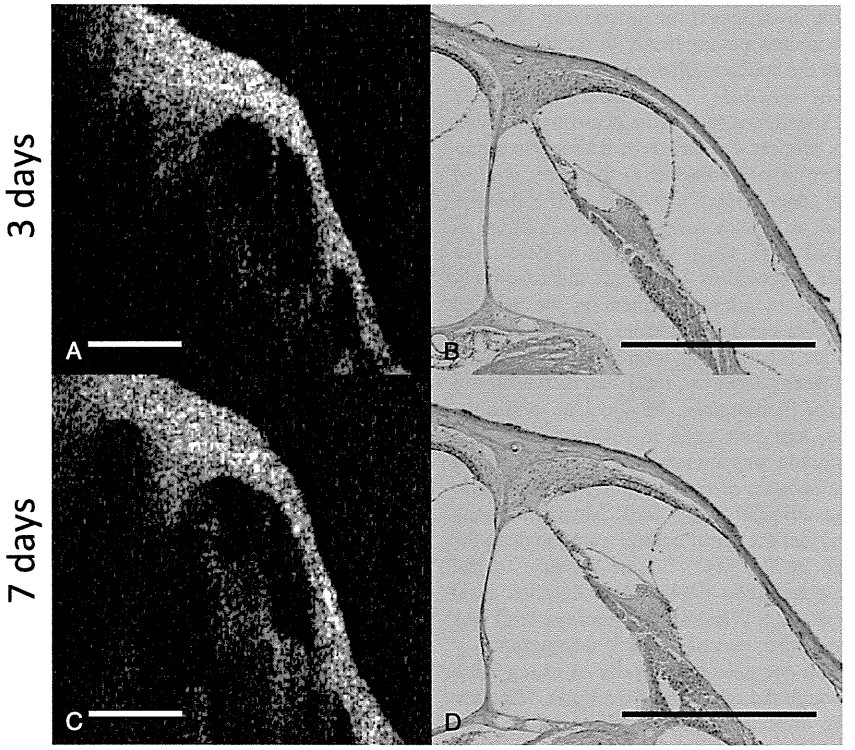

FIG. 3. Repeated visualization of the cochlea by OCT. OCT images of *Slc26a4*$^{(+/+)}$ mice cochlea 3 or 7 days after the first visualization (*A* and *C*, respectively) showed normally positioned Reissner's and basilar membranes. HE staining of the same cochlea (*B* and *D*, respectively) showed no endolymphatic hydrops and no obvious infiltration of inflammatory cells in the middle ear mucosa and inner ear. Scale bars = 500 μm.

the scala vestibuli, as shown in the OCT images. The basilar membrane was adjacent to the bony wall of the scala tympani. The spiral ligament was thinner (Fig. 2K) than that of *Slc26a4*$^{(+/+)}$ and *Slc26a4*$^{(+/-)}$ mice (Fig. 2, G and I), and the outer hair cells in the organ of Corti were degenerated (Fig. 2L). These findings were not observed using OCT (Fig. 2C) and were consistent with those of a previous report (17,19,20).

Repeated Observation of the Cochlea Using OCT

All the mice were alive at 3 or 7 days after the first visualization of the cochlea in *Slc26a4*$^{(+/+)}$ mice using OCT. The mice were anesthetized, and the middle ear was reopened. No obvious infectious pus was present in the middle ear. After the removal of the fibrin clots, OCT images were successfully obtained (Fig. 3, A and C). The intracochlear morphology, including the position of Reissner's and basilar membranes, was normal in all the OCT images. After OCT imaging, each cochlea was removed and processed for histologic assessment. In the HE images, there was no dilatation of the scala media and no obvious inflammatory cell infiltration in the middle ear mucosa and the inner ear (Fig. 3, B and D).

DISCUSSION

In this study, we investigated the potential of OCT for the analysis of cochlear pathogenesis by examining its ability to illustrate the cochlear phenotype of *Slc26a4*$^{(-/-)}$ mice in vivo. The *Slc26a4*$^{(-/-)}$ mice were completely deaf, and the HE specimens revealed a decreased number of cochlear turns, marked convexity of Reissner's membranes, basilar membranes adjacent to the bony wall of the scala tympani, degenerated hair cells, and a thinned spiral ligament, all of which were the same findings as previously reported (17). OCT was able to detect the decreased number of cochlear turns and the extremely distended Reissner's membrane, indicating the marked dilatation of the scala media. Therefore, OCT is considered a useful device for the evaluation of endolymphatic hydrops in living mice. However, OCT had difficulties in showing the basilar membranes, the cochlear modiolus, the spiral limbus, and hair cells in *Slc26a4*$^{(-/-)}$ mice. The basilar membrane was invisible in OCT images of *Slc26a4*$^{(-/-)}$ mice because of the proximity of the basilar membrane to the adjacent bony wall. Meanwhile, the cochlear modiolus and the spiral limbus were too deep for OCT to visualize in *Slc26a4*$^{(-/-)}$ mice because of the limitation of the penetration depth. More detailed axial resolution at a greater depth (additional micrometers) was needed to evaluate the extent of hair cell degeneration.

In this study, the cochlear bony walls of living mice were exposed through the removal of the bulla. Mice are known to survive after the removal of the bulla, even when followed by cell transplantation (21,22). Furthermore, we showed that repeated visualization of the cochlea in living mice 3 or 7 days after the first visualization was possible by this method without inducing endolymphatic hydrops, otitis media, or labyrinthitis. Thus, this strategy can be used, for example, in the evaluation of dynamic changes in the inner ear of living animals that have received a particular drug to induce or reduce endolymphatic hydrops.

MRI and micro-CT are the other imaging modalities capable of visualizing the detailed inner structures inside the cochlea. MRI has been already applied to humans and is able to illustrate much deeper views than OCT. In addition, MRI has the ability to reveal the area of the scala media by enhancing the signal from the perilymph by intratympanic or systemic administration of a contrast agent (1–3). However, MRI is unable to show minute structures such as Reissner's membrane because its axial resolution is about 0.5 to 1.0 mm. Moreover, the use of contrast agents contains the risk of inner ear impairment when administered locally and the possibility of nephrogenic systemic fibrosis when administered systemically (23). Although micro-CT has an axial resolution of about 1 to 100 μm (24), this method is not acceptable for living animals because of the serious tissue damage that results from the high-dose ionizing radiation (25).

The thick cochlear bony capsule in humans is an obstacle to the clinical application of OCT as a cochlear imaging modality; however, we believe that OCT can be applied in humans at least for the visualization of the endolymphatic hydrops in the lower part of the cochlea or the vestibule by visualization through the round window membrane, which is accessible through tympanostomy using a side-viewing OCT fiber (26). OCT is also available for experimental use. A previous report from Kimura and Schuknecht (27) demonstrated that obliteration of the endolymphatic sac in guinea pigs was capable of producing endolymphatic hydrops. Moreover, various procedures to elicit inner ear autoimmune disease have been reported. (28,29) The extent of endolymphatic hydrops in both models were only evaluated in samples obtained after the animals were sacrificed. OCT enables the sequential visualization of endolymphatic hydrops without sacrificing the animals. Therefore, OCT is applicable for the evaluation of various drugs for the treatment of Ménière's disease.

The present findings demonstrate that OCT can be used to evaluate the gross anatomy of mouse cochlea, including the location of Reissner's membrane and the basilar membrane. The use of OCT contributes to the evaluation of pathologic changes in the cochlea of living mice.

Acknowledgments: The authors thank Konrad Noben Trauth, Andrew Griffith, and Eric Green at the National Institute of Health (NIH) and Tsutomu Nakashima at the Department of Otorhinolaryngology, Nagoya University Graduate School of Medicine, for the generous donation of *Slc26a4*-disrupted mice.

REFERENCES

1. Zou J, Poe D, Bjelke B, Pyykkö I. Visualization of inner ear disorders with MRI in vivo: from animal models to human application. *Acta Otolaryngol Suppl* 2009;22–31.
2. Naganawa S, Satake H, Iwano S, Fukatsu H, Sone M, Nakashima T. Imaging endolymphatic hydrops at 3 Tesla using 3D-FLAIR

with intratympanic Gd-DTPA administration. *Magn Reson Med Sci* 2008;7:85–91.
3. Sano R, Teranishi M, Yamazaki M, et al. Contrast enhancement of the inner ear in magnetic resonance images taken at 10 minutes or 4 hours after intravenous gadolinium injection. *Acta Otolaryngol* 2012;132:241–6.
4. Santi PA. Light sheet fluorescence microscopy: a review. *J Histchem Cytochem* 2011;59:129–38.
5. Kopecky BJ, Duncan JS, Slliott KL, Fritzsch B. Three-dimensional reconstructions from optical sections of thick mouse inner ears using confocal microscopy. *J Microsc* 2012;248:292–8.
6. Fujimoto JG, Farkas D. *Biomedical Optical Imaging*. Oxford, UK: Oxford University Press, USA, 2009.
7. Huang D, Swanson EA, Lin CP, et al. Optical coherence tomography. *Science* 1991;254:1178–81.
8. Spaide RF, Koizumi H, Pozonni MC. Enhanced depth imaging spectral-domain optical coherence tomography. *Am J Ophthalmol* 2008;146:496–500.
9. Shah SU, Kaliki S, Shields CL, Ferenczy SR, Harmon SA, Shields JA. Enhanced depth imaging optical coherence tomography of choroidal nevus in 104 cases. *Ophthalmology* 2012;119:1066–72.
10. Collier T, Arifler D, Malpica A, Follen M, Richards-Kortum R. Determination of epithelial tissue scattering coefficient using confocal microscopy. *IEEE J Sel Top Quantum Electron* 2003;9:307–13.
11. Pierce MC, Strasswimmer J, Park BH, Cense B, de Boer JF. Advances in optical coherence tomography imaging for dermatology. *J Investig Dermatol* 2004;123:458–63.
12. Unal G, Carlier SG. In-vivo optical coherence tomography image analysis. *Biomedical Imaging: From Nano to Macro, 2010 IEEE International Symposium on* 2010;1409–10.
13. Wong BJF, Zhao Y, Yamaguchi M, Nassif N, Chen Z, de Boer JF. Imaging the internal structure of the rat cochlea using optical coherence tomography at 0.827 microm and 1.3 microm. *Otolaryngol Head Neck Surg* 2004;130:334–8.
14. Lin J, Staecker H, Jafri MS. Optical coherence tomography imaging of the inner ear: a feasibility study with implications for cochlear implantation. *Ann Otol Rhinol Laryngol* 2008;117:341–6.
15. Subhash HM, Davila V, Sun H, Nguyen-Huynh AT, Nuttall AL, Wang RK. Volumetric in vivo imaging of intracochlear microstructures in mice by high-speed spectral domain optical coherence tomography. *J Biomed Opt* 2010;15:036024.
16. Gao SS, Xia A, Yuan T, et al. Quantitative imaging of cochlear soft tissues in wild-type and hearing-impaired transgenic mice by spectral domain optical coherence tomography. *Opt Express* 2011;19:15415–28.
17. Everett LA, Belyantseva IA, Noben-Trauth K, et al. Targeted disruption of mouse Pds provides insight about the inner-ear defects encountered in Pendred syndrome. *Hum Mol Genet* 2001;10:153–61.
18. Kada S, Nakagawa T, Ito J. A mouse model for degeneration of the spiral ligament. *J Assoc Res Otolaryngol* 2009;10:161–72.
19. Everett LA, Glaser B, Beck JC, et al. Pendred syndrome is caused by mutations in a putative sulphate transporter gene (PDS). Nat Genet. *Nature Publishing Group* 1997;17:411–22.
20. Wangemann P, Itza EM, Albrecht B, et al. Loss of KCNJ10 protein expression abolishes endocochlear potential and causes deafness in Pendred syndrome mouse model. *BMC Med* 2004;2:30.
21. Sharif S, Nakagawa T, Ohno T, et al. The potential use of bone marrow stromal cells for cochlear cell therapy. *Neuroreport* 2007;18:351–4.
22. Nishimura K, Nakagawa T, Sakamoto T, Ito J. Fates of murine pluripotent stem cell-derived neural progenitors following transplantation into mouse cochleae. *Cell Transplant* 2012;21:763–71.
23. Goenka AHA, Das CJC, Sharma RR. Nephrogenic systemic fibrosis: a review of the new conundrum. *Natl Med J India* 2009;22:302–6.
24. Li XX, Anton NN, Zuber GG, et al. Iodinated α-tocopherol nanoemulsions as non-toxic contrast agents for preclinical X-ray imaging. *Biomaterials* 2012;34:481–91.
25. Saito S, Murase K. Detection and early phase assessment of radiation-induced lung injury in mice using micro-CT. *PLoS ONE* 2012;7:e45960.
26. Wu Y, Xi J, Huo L, et al. Robust high-resolution fine OCT needle for side-viewing interstitial tissue imaging. *IEEE J Sel Top Quantum Electron* 2010;16:863–9.
27. Kimura RS, Schuknecht HF. Membranous hydrops in the inner ear of the guinea pig after obliteration of the endolymphatic sac. *Pract Otorhinolaryngol (Basel)* 1965;27:343–54.
28. Gates GAG. Ménière's disease review 2005. *J Am Acad Audiol* 2005;17:16–26.
29. Tomiyama SS. Development of endolymphatic hydrops following immune response in the endolymphatic sac of the guinea pig. *Acta Otolaryngol* 1991;112:470–8.

Otology & Neurotology
33:886–890 © 2012, Otology & Neurotology, Inc.

Type 1 Allergy-Induced Endolymphatic Hydrops and the Suppressive Effect of Leukotriene Receptor Antagonist

*Taizo Takeda, †Setsuko Takeda, ‡Naoya Egami, ‡§Akinobu Kakigi, §Rie Nishioka, and ‡Tatsuya Yamasoba

**Department of Otolaryngology, Nishinomiya Municipal Central Hospital; †Nishinomiya; ‡Department of Otolaryngology, Faculty of Medicine, University of Tokyo, Tokyo; and §Department of Otolaryngology, Kochi Medical School, Kochi, Japan*

Objective: To investigate allergic endolymphatic hydrops (EH) and the effect of leukotriene receptor antagonist (LTRA).
Methods: Experiment 1: Thirty-six guinea pigs were actively sensitized with DNP-ascaris twice and were provoked with DNP–bovine serum albumin 1 week after the second sensitization. Alterations in the inner ear were investigated histologically at 1, 12, 24, and 36 hours after the provocation, and changes of the endolymphatic space were quantitatively assessed. The animals in the control group received no sensitization but only distilled water. **Experiment 2**: Twenty-four guinea pigs were actively sensitized and provoked in the same manner. Animals received oral administration of LTRA 1 hour before the provocation. Alterations in the inner ear were investigated as same manner as in Experiment 1. **Experiment 3**: Eleven of 19 guinea pigs were actively sensitized and provoked in the same manner. Eight animals in the control group received distilled water. One hour after these procedures, the changes in p-AVP levels were investigated.
Results: Experiment 1: EH was observed 12, 24, and 36 hours after the last sensitization. In these groups, their cross-sectional areas of the scala media were significantly larger than that of the control group. Degranulation of mast cells was observed in the endolymphatic sac. **Experiment 2**: In animal groups with LTRA, EH was not observed at all. **Experiment 3**: P-AVP levels were significantly elevated in animals with the sensitization.
Conclusion: The sensitization with DNP-Ascaris produced allergic EH and elevation of p-AVP, and allergic EH was inhibited by LTRA. **Key Words:** Endolymphatic hydrops—Leukotriene receptor antagonist—Type 1 allergy—Vasopressin.

Otol Neurotol **33**:886–890, 2012.

Since Duke's (1) report in 1923, several clinical reports have suggested allergy as a causative or associated factor in the cause of inner ear disorders, especially Ménière's disease or endolymphatic hydrops (EH) (2–4). These reports were mainly based on clinical documentation that vertigo, tinnitus, and hearing loss in Ménière's disease were improved after desensitization to inhalant allergens and an elimination diet for food allergies.

Furthermore, Derebery and Berliner (4) reported a high incidence of allergic symptoms in patients with Ménière's disease and a much higher incidence of bilaterality in cases with allergic symptoms than in the general population is typically reported. The existence of the endolymphatic sac as a target organ of the allergic reaction has been proposed as a possible mechanism underlying inner ear symptom (5,6).

Meanwhile, allergic insults are known to result in elevated plasma arginine vasopressin (p-AVP) levels (7–10). Because the endolymphatic volume experimentally increases by an elevation in p-AVP (11), it is likely that AVP participates in a mechanism underlying the relationship between allergy and the development of EH.

In the present study, guinea pigs were sensitized and challenged with dinitrophenylated-Ascaris (DNP-As) antigen. The influence of the allergic reaction induced by DNP-As challenge on the inner ear and inhibition effects of a leukotriene receptor antagonist (LTRA) were morphologically investigated. Changes of p-AVP levels also were examined.

MATERIALS AND METHODS

Experiment 1

Thirty-six guinea pigs were actively sensitized with DNP-As twice at an interval of 1 month, and were provoked with an

Address correspondence and reprint requests to Akinobu Kakigi, M.D., Department of Otolaryngology, Faculty of Medicine, Tokyo University, 7-3-1, Hongo, Bunkyo-ku, Tokyo, 113-8655, Japan; E-mail: kakigia@gmail.com

The authors disclose no conflicts of interest.

injection of DNP-BSA (bovine serum albumin) and DNP-As 1 week after the second sensitization. The alterations in the inner ear were investigated histologically at 1, 12, 24, and 36 hours after the provocation. Ten animals served as a control group, receiving no sensitization but only distilled water. For the quantitative assessment of changes of the endolymphatic space, the cross-sectional area of the scala media was measured from the mid-modiolar sections of the cochlea. The assessment of volumetric changes of the endolymphatic space was conducted as shown in Figure 1. The measurement was performed essentially as previously described (11).

Experiment 2

Twenty-four guinea pigs were actively sensitized in the same manner. One week after the second sensitization, animals received oral administration of LTRA (30 mg/kg of pranlukast hydrate) based on the previous report (12) and were provoked in the same manner 1 hour later. In Experiment 2, the alterations of the inner ear were investigated histologically at 1, 12, 24, and 36 hours after the provocation, and changes of the endolymphatic space were quantitatively assessed. In Experiments 1 and 2, histologic study was fundamentally conducted by light microscopy with hematoxylin-eosin staining. Also, to investigate the degranulation of the mast cells, species of the endolymphatic sac were stained with toluidine blue.

Experiment 3

Eleven of 19 guinea pigs were actively sensitized and provoked in the same manner. Four of them received premedication with LTRA. The remaining 8 animals, which served as controls, only received the subcutaneous injection of distilled water. One hour after these procedures, all animals were killed for the measurement of p-AVP concentrations. Blood samples were generally collected at around 6 AM, while animals were under light anesthesia established by an intramuscular injection of xylazine (5 mg/kg) and ketamine (35 mg/kg). The animals were quickly decapitated at 0 minute with the use of a guillotine, and trunk blood was collected in plastic tubes containing ethylenediamine tetra-acetic acid–Na. The blood volume collected was not less than 10 ml. Partly to avoid contamination of platelet AVP, and partly to avoid degradation of AVP activity resulting from its short half-life, blood samples were immediately centrifuged at 4°C, and plasma was stored at -20°C until analyzed for AVP. P-AVP concentrations were measured by a radioimmunoassay of plasma extracted using C_{18} Sep-Pak cartridges (Water Associates, Milford, MA, USA). The extracts were evaporated under a stream of air overnight. Analysis of AVP was performed with the use of the AVP-RIA kit "Mitsubishi"

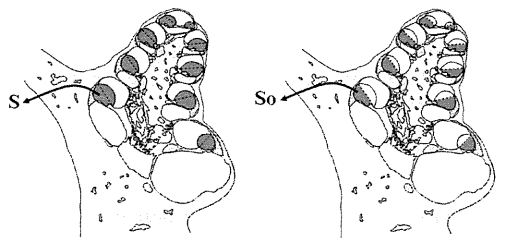

FIG. 1. Quantitative analysis of increase ratio (IR) of the scala media.

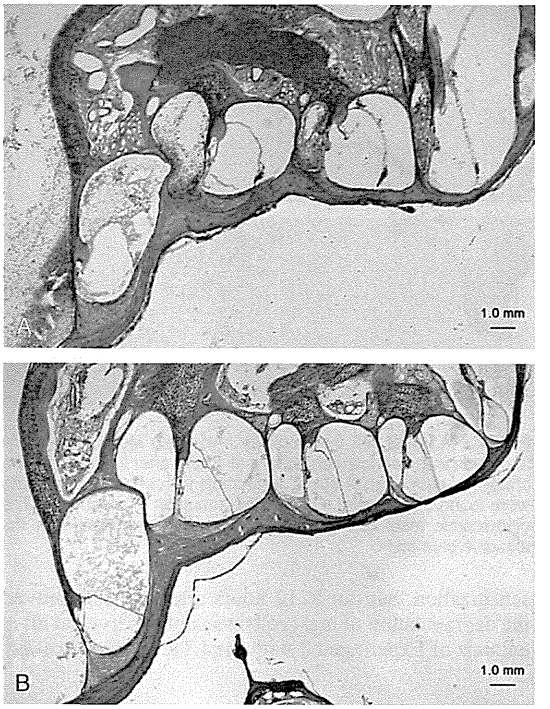

FIG. 2. Allergy-induced EH. Systemic challenge with DNP-As induced the development of EH at 12, 24, and 36 hours after the last immune challenge but not at 1 hour. Figure 2 A shows a typical image of the cochlea 12 hours after the last challenge with DNP-As. However, premedication with LRA inhibited the development of EH (Fig. 2B).

(Mitsubishi Chemical Co., Tokyo, Japan). The detailed assay procedure was described previously (11).

The care and use of animals in this study were approved by the Kochi Medical School Animal Care and Use Committee.

RESULTS

Histologic Finding

Figure 2 A shows a typical image of the cochlea 12 hours after the last sensitization in the animal group of Experiment 1. Reissner's membrane was remarkably extended, and EH was evident in all turns. Similar EH also was observed 24 and 36 hours after the last sensitization but not after 1 hour. However, the development of EH was not observed in any animals of Experiment 2 with LTRA premedication, as shown in Figure 2B. As to the histologic changes of the endolymphatic sac, cells with large basophilic granules (Fig. 3A) were observed in the lumen of the endolymphatic sac 1 hour after the last sensitization in the animal group of Experiment 1. Because these granules were well stained by toluidine blue (Fig. 3B), the cells expressed within the endolymphatic sac were thought to be mast cells with degranulation. Mast cells appeared only at 1 hour after the last

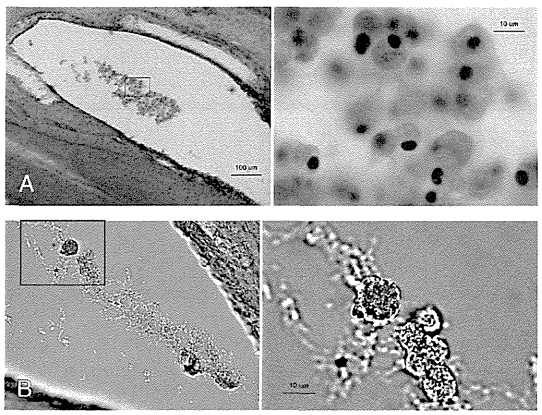

FIG. 3. *A,* Mast cell (hematoxylin and eosin stain), Mast cells appeared in the endolymphatic sac at 1 hour after the last immune challenge but not at 12 hours. In animals with LRA, no mast cells were found (not shown). *B,* The degranulation of mast cells. The cytoplasmic mast cell granules show metachromasia with the toluidine blue stain.

sensitization, but not at 12 hours after then. Moreover, the degranulation of mast cells was not observed at all in animals of Experiment 2 with the LTRA premedication.

Assessment of Volumetric Change of the Scala Media

The results of the quantitative analysis of the increase ratios (IRs) of the cross-sectional area of the scala media and significance levels are presented in Figure 4. In Experiment 1 without LTRA premedication, the mean values of IRs were larger in groups at 12, 24, and 36 hours than those in the control and 1-hour groups. Statistical analysis revealed that there was no significant difference between the control group and 1 hour group or among the 3 groups of 12, 24, and 36 hours ($p > 0.1$ by 1-way analysis of variance [ANOVA]) but that there were significant differences between each of the control and 1-hour groups and each of the 12-, 24-, and 36-hour groups ($p < 0.05$, ANOVA, Cochran-Cox test). These results support that systemic immune challenge with DNP-As antigen induced the development of EH. In contrast, the means of IRs of Experiment 2 animals with LTRA premedication were not markedly different from those of control animals. Statistically significant changes

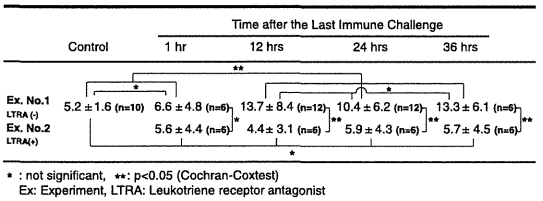

FIG. 4. Increase ratios of the cross-sectional area of the scala media.

A comparison of p-AVP levels

	Control	LTRA(+)	LTRA(-)
p-AVP (pg/ml)	1.3 ± 0.7 (n=8)	10.8 ± 6.1 (n=4)	17.1 ± 6.2 (n=6)
	p<0.01	p<0.05	
	p<0.01		

LTRA (+): DNP-As challenge with LTRA premedication
LTRA (-): DNP-As challenge without LTRA premedication

FIG. 5. A comparison of p-AVP levels.

in IRs were not observed among groups of 1, 12, 24, and 36 hours, nor between these groups and the control animals ($p > 0.1$ by 1-way ANOVA). Thus, it was confirmed that LTRA premedication inhibited the development of EH induced by the immune challenge of DSP-As.

Comparison of p-AVP Levels Among Control Animals, Sensitized Animals With LTRA Premedication, and Sensitized Animals Without LTRA Premedication

One sensitized animal developed anaphylactic-like acute dyspnea or respiratory distress within 2 minutes after the immune challenge. A blood sample was immediately collected to investigate the p-AVP level, but the datum of p-AVP level is omitted from the present study. The p-AVP levels of the remaining 18 animals (8 control and 10 sensitized animals) were statistically estimated. Figure 5 shows a comparison of *p*-AVP levels among control animals, sensitized animals with LTRA premedication and sensitized animals without LTRA premedication. Means of *p*-AVP levels were elevated in animals with the sensitization, with the mean *p*-AVP level being the highest in sensitized animals without LTRA. The ANOVA null hypothesis of equal means was rejected using the ANOVA *F*-test. Statistical analysis was carried out using Fisher's least significant difference method. The elevation in *p*-AVP levels was significant (control versus LTRA (+), control versus LTRA (-); $p < 0.01$ Fisher's LSD), and also, *p*-AVP levels were significantly different between LTRA (+) and LTRA (-) ($p < 0.05$ Fisher's LSD). These results indicated that DNP-As challenge induced an elevation in p-AVP level and that LTRA premedication reduced the elevation in p-AVP.

As to the animal discarded from the present study because of anaphylactoid reactions, the p-AVP level showed a relatively low value of 1.1 pg/ml, compared with the mean value of control animals. This result is consistent with the experimental and clinical fact that the *p*-AVP concentration decreases in anaphylactic or septic shock with vasodilatory hypotension and acute respiratory distress (13,14).

DISCUSSION

The present study was originally designed to investigate the effects of LTRA (pranlukast hydrate) on EH induced by local immune challenge to the inner ear via the stylomastoid foramen. This procedure was reported by Ishikawa's group (15–17). According to their reports,

EH developed on the challenged side of the inner ear from 12 to 48 hours after local challenge (15). In our pilot study, similar findings also were confirmed, but surprisingly, EH was observed in the opposite ear as well, which was not noted in their reports. On the basis of these findings, the present study was redesigned to investigate whether systemic immune challenge might influence the inner ear and, if any alteration occurred, whether it was caused by an allergic reaction.

In the present study, systemic immune challenge with DNP-As antigen was confirmed to provoke allergic reaction in the inner ear, which was situated at the local site. Because degranulation of mast cells was found in the endolymphatic sac 1 hour after the last immune challenge, type 1 (or immediate) hypersensitivity was thought to be responsible for the present reaction. The immune challenge also produced EH 12 hours or later after the provocation. The development of EH was inhibited by premedication with LTRA (pranlukast hydrate). Therefore, EH is thought to result from allergic reactions. As to the mechanism underlying the development of EH, one possible factor is the release of chemical mediators, including histamine, serotonin, heparin, leukotriene, and so on, from mast cells in the endolymphatic sac. Because the endolymphatic sac is a key site not only in the inner ear immune defense (5,6) but also in the secretion and absorption of endolymph (18), chemical mediators released from mast cells might produce disturbances of the inner ear fluid homeostasis in the endolymphatic sac. Although H(1), H(2), and H(3) is only known as receptors of chemical mediators in the endolymphatic sac (19),the suppressive effect of LTRA on the development of EH indicates that leukotriene plays the most contributing role in the development of EH.

The other factor is an elevation in p-AVP levels. Immune challenges, in general, activate the hypothalamic stress-related neurons through pathways that show similarities to those that are commonly recruited by other stressors. Experimentally, inducible expression of AVP genes in the parvocellular neurosecretory neurons of the paraventricular nucleus is known to have a pivotal regulatory role in the activation of HPA axis responses to different stressors, including immune challenges (9). Clinically, elevated AVP levels were reported in patients with immunologic inflammation, for example, asthma, atopic dermatitis, rheumatoid arthritis, and ankylosing spondylitis (7,8,10,20). In the present study, *p*-AVP levels were elevated by DNP-As challenge, as clinically observed in allergic diseases. Because the endolymphatic volume experimentally increases by an elevation in p-AVP, elevated *p*-AVP levels might be a causative factor for the development of EH (11). Furthermore, the premedication with LTRA inhibited the elevation in p-AVP level as well as the development of EH induced by DNP-As challenge. These results seem to indicate that elevated *p*-AVP levels are closely linked to the development of EH. However, LTRA premedication also inhibited the appearance of mast cells with degranulation in the endolymphatic sac. Thus, the present experiments cannot confirm whether the DNP-As-induced EH is caused by local allergic reactions or by systemic allergic reactions or both.

Clinically, it is unknown how many dosages in a human being correspond to 30 mg/kg of pranlukast hydrate used in the present study. The dosage is the effective dose (ED50) for antiallergic action in rat and is not so much in rodent, at least. For human, the clinically effective dosage is 450 mg/day per 60 kg. Furthermore, it is difficult fast-forwarding to humans; if it could do, LTRA might prevent EH in patients with existing and/or underlying atopy.

Although further studies are required to solve the mechanism underlying allergic EH and apply LTRA for the treatment, this is the first report of type 1 allergic EH induced by a systemic immune challenge.

CONCLUSION

Sensitization with DNP-As produced allergic EH and caused an elevation in p-AVP levels. Premedication with LTRA inhibited the development of allergic EH and the elevation of *p*-AVP. The development of EH was thought to be caused by a type 1 allergic reaction because degranulation of mast cells occurred in the endolymphatic sac.

Acknowledgments: This study was supported by a Health and Labor Science Research Grant for Research on Specific Disease (Vestibular Disorders) from the Ministry of Health, Labor, and Welfare of Japan.

REFERENCES

1. Duke WW. Meniere's syndrome caused by allergy. *JAMA* 1923; 81:2179–81.
2. Clemis JD. Allergic cochleovestibular disturbances. *Ann Allergy* 1967;27:370–8.
3. Derebery MJ. Allergic management of Meniere's disease: an outcome study. *Otolaryngol Head Neck Surg* 2000;122:174–82.
4. Derebery MJ, Berliner KI. Prevalence of allergy in Meniere's disease. *Otolaryngol Head Neck Surg* 2000;123:69–75.
5. Tomiyama S, Harris JP. The endolymphatic sac: its importance in inner ear immune responses. *Laryngoscope* 1986;96:685–91.
6. Kawauchi H, Ichimiya I, Kaneda N, Mogi G. Distribution of immunocompetent cells in the endolymphatic sac. *Ann Otol Rhinol Laryngol* 1992;101:39–47.
7. Baker JW, Yerger S, Segar WE. Elevated plasma antidiuretic hormone levels in status asthmaticus. *Mayo Clin Proc* 1976;51:31–4.
8. Dawson KP, Fergusson DM, West J, Wynne C, Sadler WA. Acute asthma and antidiuretic hormone secretion. *Thorax* 1983;38:589–91.
9. Kovács KJ. Neurohypophyseal hormones in the integration of physiological responses to immune challenges. *Prog Brain Res* 2002;139:127–46.
10. Aoki T. Serum antidiuretic hormone is elevated in relation to the increase in average total body transepidermal water loss in severe atopic dermatitis. *Br J Dermatol* 2005;153:359–63.
11. Takeda T, Takeda S, Kitano H, Okada S, Kakigi A. Endolymphatic hydrops induced by chronic administration of vasopressin. *Hearing Res* 2000;140:1–6.
12. Nakagawa N, Obata T, Kobayashi T, et al. Effect of a peptide leukotriene receptor antagonist, ONO-1078, on guinea-pig models of asthma. *Eur J Pharmacol* 1993;235:211–9.
13. Dewachter P, Jouan-Hureaux V, Lartaud I, et al. Comparison of arginine vasopressin, terlipressin, or epinephrine to correct hypotension in a model of anaphylactic shock in anesthetized brown Norway rats. *Anesthesiology* 2006;104:734–41.
14. Landry DW, Levin HR, Gallant EM, et al. Vasopressin deficiency contributes to the vasodilation of septic shock. *Circulation* 1997; 95:1122–5.

15. Miyamura K, Kanzaki Y, Nagata M, Ishikawa T. Provocation of nystagmus and deviation by type I allergy in the inner ear of the guinea pig. *Ann Allergy* 1987;58:36–40.
16. Uno K, Miyamura K, Kanzaki Y, Fukuda H, Masuyama K, Ishikawa T. Type I allergy in the inner ear of the guinea pig. *Ann OtolRhinolLaryngol Suppl* 1992;157:78–81.
17. Uno K, Miyamura K, Kanzaki Y, Fukuda H, Masuyama K, Ishikawa T. Audiological study in guinea pigs with type I allergy induced in the inner ear. *Ann OtolRhinolLaryngol* 1993;102:537–42.
18. Couloigner V, Teixeira M, Sterkers O, Rask-andersen H, Ferrary E. Le sac endolymphatique: sesfonctions au sein de l'oreille intern. *Medecine science* 2004;20:304–10.
19. Dagli M, Goksu N, Eryilmaz A, et al. Expression of histamine receptors (H(1), H(2), and H(3)) in the rabbit endolymphatic sac: an immunohistochemical study. *Am J Otolaryngol* 2008;29:20–3.
20. Chinkanza IC, Petrou p, Chrousos G. Pertubations of arginine vasopressin secretion during inflammatory stress. Pathophysiologic implication. *Ann N Y Acad Sci* 2000;917:825–34.

Acta Oto-Laryngologica, 2011; Early Online, 1–8

informa
healthcare

ORIGINAL ARTICLE

Endolymphatic hydrops in Meniere's disease detected by MRI after intratympanic administration of gadolinium: Comparison with sudden deafness

ARATA HORII[1,2], YASUHIRO OSAKI[2], TADASHI KITAHARA[2], TAKAO IMAI[2], ATSUHIKO UNO[2], SUETAKA NISHIIKE[2], NORIHIKO FUJITA[3] & HIDENORI INOHARA[2]

[1]*Department of Otolaryngology, Suita Municipal Hospital,* [2]*Department of Otorhinolaryngology-Head and Neck Surgery, Osaka University Graduate School of Medicine and* [3]*Department of Radiology, Osaka University Graduate School of Medicine, Osaka, Japan*

Abstract

Conclusion: The detection rate of endolymphatic hydrops was significantly higher in patients with Meniere's disease compared with those with sudden deafness, indicating that 3 T magnetic resonance imaging (MRI) with intratympanic gadolinium injection was effective in diagnosing endolymphatic hydrops. *Objectives:* To compare the detection rate of endolymphatic hydrops between patients with Meniere's disease and sudden deafness as controls by 3 T MRI after intratympanic gadolinium injection with conventional pulse sequence such as two-dimensional fluid-attenuated inversion recovery. *Methods:* Ten patients with unilateral Meniere's disease and eight with sudden deafness underwent inner ear MRI 24 h after intratympanic gadolinium injection. *Results:* The endolymphatic space was detected as a low signal intensity area, while the perilymphatic space showed high intensity by gadolinium enhancement. Due to faint enhancement, images could not be evaluated in 1 of 10 patients with Meniere's disease. However, the other nine patients together with two of the eight with sudden deafness were diagnosed as having hydrops. The difference in detection rates between the two diseases was statistically significant. Two hydrops-positive cases with sudden deafness were considered to be of the secondary type of hydrops, because images were taken after partial recovery from hearing loss several months after the onset of the disease.

Keywords: *Radiological diagnosis, contrast enhancement, secondary hydrops, 3 T MRI*

Introduction

According to the guidelines for diagnosing and grading the severity of Meniere's disease established by the American Academy of Otolaryngology-Head and Neck Surgery (1995), 'definite' or 'certain' Meniere's disease can be diagnosed only after post-mortem histological confirmation of endolymphatic hydrops [1]. However, strong suspicion of endolymphatic hydrops can be established on the basis of the following findings: dominant -summating potential/action potential (-SP/AP) on electrocochleogram (EcochG), hearing improvement on glycerol test, and vestibulo-ocular reflex (VOR) gain increase after furosemide administration [2]. The former two methods cannot be performed in patients with profound hearing loss, while the latter one cannot separately evaluate the function of the right and left canals.

The diagnosis of endolymphatic hydrops by image analysis is established on the basis of visualization of the Reissner's membrane or discrimination of endolymph from perilymph. Indeed, the Reisner's membrane could be visualized in guinea pig cochleas by inner ear magnetic resonance imaging (MRI) using a 7.1 T MR unit [3,4], whereas an experimental gadolinium (Gd)-enhanced 4.7 T MRI could discriminate the perilymphatic and endolymphatic spaces in live guinea pigs [5,6]. However, technical and safety

Correspondence: Dr Arata Horii MD PhD, Department of Otolaryngology, Suita Municipal Hospital, 2-13-20 Katayama-Cho, Suita, Osaka 564-0082, Japan. Tel: +81 6 6387 3311. Fax: +81 6 6380 5825. E-mail: ahorii@ent.med.osaka-u.ac.jp

(Received 28 October 2010; accepted 10 December 2010)

ISSN 0001-6489 print/ISSN 1651-2251 online
DOI: 10.3109/00016489.2010.548403

issues limit application of these methods to patients. Recently, 3 T MRI in combination with intratympanic administration of gadolinium has been reported to successfully visualize the endolymphatic hydrops in patients with Meniere's disease [7–10]. However, control studies with normal volunteers or patients with other inner ear diseases have not been conducted. Moreover, the previous studies used a Siemens 3 T MR unit with three-dimensional fluid-attenuated inversion recovery (3D-FLAIR) or three-dimensional real inversion recovery (3D-real IR) sequences [7–10]. This combination of MR unit and pulse sequences is a relatively unique and novel one, which is not available to most institutions worldwide, explaining why this useful technique is not widely disseminated. The aims of this paper were first to compare the detection rate of endolympatic hydrops between patients with Meniere's disease and those with sudden deafness by analyzing images taken by a General Electric (GE) 3 T MR unit after intratympanic gadolinium injection with conventional sequence such as two-dimensional FLAIR (2D-FLAIR) and second to demonstrate the existence of secondary hydrops following sudden deafness by radiological techniques.

Material and methods

This study was conducted under approval by the Ethical Committee of Osaka University Hospital (IRB# 08223).

Ten patients suffering from unilateral Meniere's disease and eight with sudden deafness underwent MRI in combination with intratympanic injection of gadolinium. The diagnosis of Meniere's disease and sudden deafness was based on criteria established by the Japan Equilibrium Society and the Ministry of Health, Labor, and Welfare of Japan. Cases of low-tone sudden deafness were excluded from this study. Patients with Meniere's disease or sudden deafness were subjected to an intratympanic injection therapy of gentamicin or steroid, respectively following endolymphatic image analyses. Gadodiamide hydrate (Omniscan®) diluted eightfold in saline was injected intratympanically using a 23 gauge needle and syringe. At 24 h after the injection, axial images were taken by 3 T GE MR unit with fast imaging employing steady-state acquisition (FIESTA) and 2D-FLAIR sequences. As images taken with FIESTA sequence were quite similar to those taken with constructive interference in the steady-state (CISS) sequence used in previous studies [7–10], FIESTA images are referred to as CISS images in this study. The parameters for CISS (FIESTA) were as follows: TR of 7.7 ms, TE of 3.2 ms, flip angle of 50°C, matrix size of 384 × 384 (interpolated to 512 × 512), slice thickness of 1 mm (interpolated to 64 axial images at 0.5 mm increments), and a 16 cm square field of view. The parameters for 2D-FLAIR were as follows: TR of 9000 ms, TE of 125 ms, TI of 2500 ms, matrix size of 384 × 384 (interpolated to 512 × 512), and 14 axial 2 mm thick slices covering the labyrinth with a 16 cm square field of view. The number of excitations was two, and the scan time was 10 min. The dilution ratio of gadolinium and the interval between Gd injection and MR examination were optimized as in previous reports [7,9].

CISS sequences are suitable for the detection of the outline of the whole inner ear, because they are heavily T2-weighted images and thus sensitive to both the endolymph and perilymph. In contrast, intratympanically injected Gd can enter only into the perilymphatic space, leaving the endolymph with no or only a faint gadolinium enhancement, which explains the good contrast between the perilymph and endolymph in FLAIR sequences [7]. Indeed, by comparing the 2D-FLAIR and CISS images, it was possible to easily visualize both the endolymphatic hydrops and inner ear structures. Two of the authors (A.H. and Y.O.) independently examined the MR images without knowledge of the diagnosis of probable endolymphatic hydrops. Existence of endolymphatic hydrops was examined in the cochlea and vestibule according to the grading system for endolymphatic hydrops using MRI proposed by Nakashima et al. [11]. For semicircular canals, endolymphatic hydrops was diagnosed if the ratio of the area of the endolymphatic space to that of the fluid space (sum of the endolymphatic and perilymphatic space) exceeded 33.3%. In case of a disagreement on the radiological diagnosis, a discussion was held between the two examiners for a concerted final judgment.

An EcochG was recorded from the external auditory canal and an -SP/AP ratio of >0.4 was considered a sign of endolymphatic hydrops. Bithermal caloric tests were performed to evaluate the vestibular function. The percentage of canal paresis (CP%) was calculated using the Jongkees formula: 0% indicating the absence of right–left differences, whereas 100% was indicative of total canal paresis. The difference between the rate of hydrops-positive cases in patients with Meniere's disease and those with sudden deafness was tested with Fisher's exact test and a p value < 0.05 was considered significant.

Results

Using 2D-FLAIR sequences, the endolymphatic space could be detected as a low or no signal intensity

area, while the perilymphatic space was shown as a high intensity area due to gadolinium enhancement (Figures 1–3). When assessing FLAIR images, CISS images in the same plane were always helpful in identifying inner ear structures (Figures 1–3). Numbers in Figures 1–3 indicate the patient ID numbers.

Figure 1 shows representative images of hydrops-positive (Figure 1A and B) and hydrops-negative (Figure 1C and D) cochlea in FLAIR and CISS images. As shown in FLAIR images in Figure 1A and B, enlarged scala media of the basal turn (arrows) was seen as a low or no signal intensity area surrounded by perilymphatic space, which appeared as a high signal intensity area due to gadolinium enhancement. Thus, endolymphatic hydrops of the cochlear basal turn appeared as a scallop-like shape. In contrast, as shown in FLAIR images in Figure 1C and D, no remarkable low signal intensity area was found in cochlear basal turns (arrows), indicating a hydrops-negative cochlea.

Figure 2 shows representative images of hydrops-positive (Figure 2A and B) and hydrops-negative (Figure 2C and D) in cross-sectional FLAIR and CISS images of vertical canals. In the FLAIR images in Figure 2A and B, enlarged endolymphatic spaces of posterior (Figure 2A) and anterior (Figure 2B) canals were seen as low or no signal intensity area (arrows) surrounded by perilymphatic spaces with Gd-enhanced high signal intensity. In contrast, as shown in FLAIR images in Figure 2C and D, no remarkable low signal intensity area was found in the posterior (Figure 2C) and anterior (Figure 2D) canals, indicating hydrops-negative canals.

Figure 3 shows representative images of hydrops-positive (Figure 3A and B) and hydrops-negative (Figure 3C and D) vestibule and lateral canal in FLAIR and CISS images. FLAIR images in Figure 3A and B show enlarged endolymphatic space of the vestibule (Figure 3A) and lateral canal (Figure 3B), which appear as low or no signal intensity area (arrows) surrounded by perilymphatic spaces with Gd-enhanced high signal intensity. In contrast, as shown in FLAIR images in Figure 3C and D, no remarkable low signal intensity area was found in the vestibule (Figure 3C) and lateral canal (Figure 3D), indicating hydrops-negative structures.

Table I summarizes the patients' profiles and locations of endolymphatic hydrops. It was not possible to evaluate the endolymphatic images in 1 of the 10 patients with Meniere's disease due to poor contrast enhancement (patient no. 1). However, we could assess the endolymphatic hydrops in nine patients with Meniere's disease and eight with sudden deafness. The finding of hydrops in at least one portion of the inner ear was diagnosed as endolymphatic hydrops in that patient. All of nine patients with Meniere's disease and two of eight patients with sudden deafness were diagnosed as having

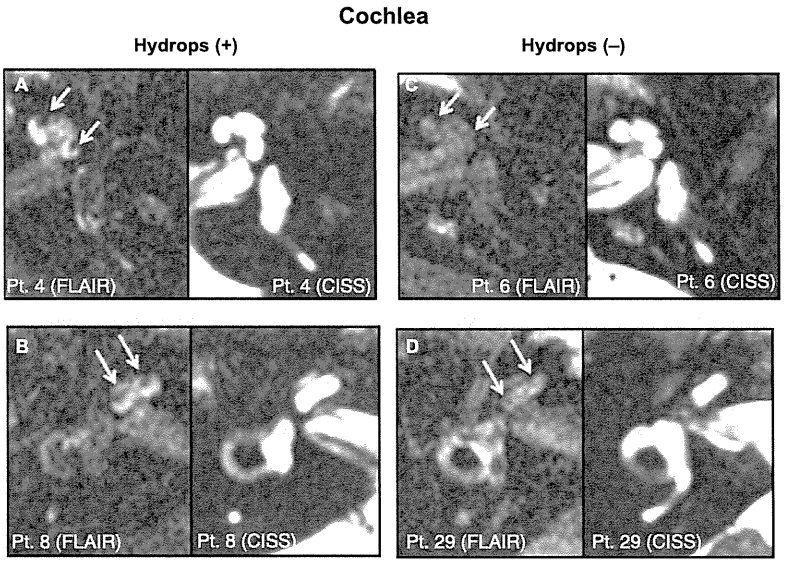

Figure 1. Hydrops-positive (A and B) and hydrops-negative (C and D) cochlea in 2D-FLAIR and CISS images. (A and B) 2D-FLAIR images show enlarged scala media of basal turn (arrows); endolymphatic hydrops is seen as scallop-like shape with low or no signal intensity area surrounded by perilymphatic spaces showing high signal intensity area due to gadolinium enhancement. (C and D) 2D-FLAIR images: no remarkable low signal intensity area was found in cochlear basal turns (arrows). CISS images in the same plane were helpful in identifying inner ear structures. Numbers in the figures indicate patient ID numbers.

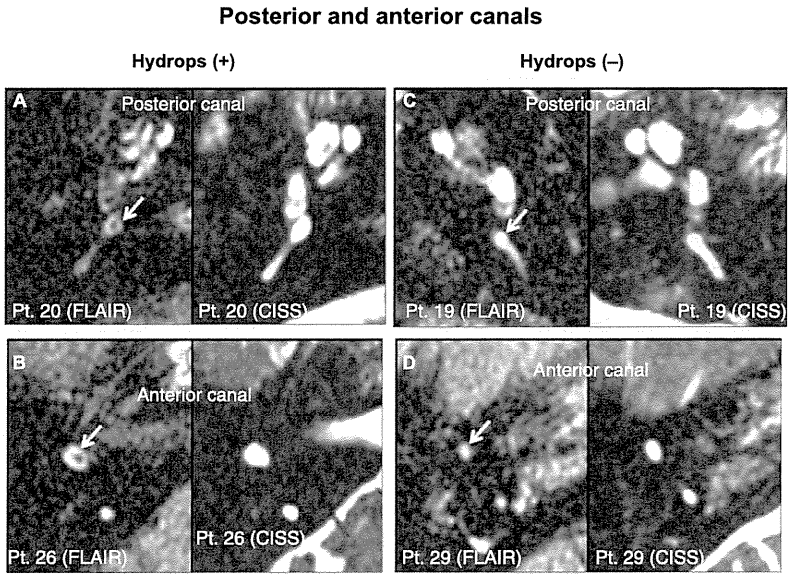

Figure 2. Hydrops-positive (A and B) and hydrops-negative (C and D) vertical canals in 2D-FLAIR and CISS images. (A and B) In 2D-FLAIR images, cross-sectional images showing an enlarged endolymphatic space of the posterior (A) and anterior (B) canals are seen as low or no signal intensity area (arrows) surrounded by perilymphatic spaces that are seen as high signal intensity area due to gadolinium enhancement. (C and D) In 2D-FLAIR images, no remarkable low signal intensity area was found in the posterior (C) and anterior (D) canals. CISS images in the same plane were helpful in identifying inner ear structures. The numbers in the figures indicate the patient ID numbers.

endolymphatic hydrops (Figure 4). The difference in detection rates between the two groups was statistically significant (Fisher's exact test, $p = 0.002262$). Endolymphatic hydrops was noted in the cochlea in 8 of 9 patients with Meniere's disease, whereas only 6 of 10 patients had dominant -SP/AP in EcochG (Table I). Ipsilateral caloric weakness (CP% $\geq$ 24%) was noticed in all of 10 patients with Meniere's disease, while 7 of 9 patients had endolymphatic hydrops in lateral canals (Table I). Endolymphatic hydrops in patients with Meniere's disease was most often observed in the cochlea, vestibule, and posterior canal, followed by the lateral and anterior canal (Table I).

In hydrops-positive cases of sudden deafness (patient nos 17 and 21), a detailed chart review revealed that MR images of these two patients were taken after partial recovery from hearing loss 11 and 2 months after the onset of disease, respectively. Six of eight patients with sudden deafness did not develop endolymphatic hydrops 1–7 months after the onset of hearing loss.

Discussion

To the best of our knowledge, this is the first systemic study to conduct control studies with non-Meniere's patients to evaluate inner ear MRI with intratympanic Gd injection. Although animal studies using guinea pigs demonstrated that intratympanic injection of gadolinium affected neither the endocochlear potential nor the morphology of the stria vascularis [12], it has been difficult for researchers to undertake control studies using healthy volunteers due to ethical problems. In the present study, we used patients with sudden deafness as controls and excluded those with low-tone sudden deafness, which is sometimes the first manifestation of Meniere's disease [13]. In this regard, sudden deafness might not be a perfect control disease, because the pathophysiology of this clinical entity may be multifocal and is still not fully understood. However, the fact that the rate of endolymphatic hydrops-positive patients was significantly higher in patients with Meniere's disease as compared with those with sudden deafness, strongly suggests that radiological diagnosis of endolymphatic hydrops with this method is accurate and useful in clinical settings. As limitations of this study, the number of patients in each group was not large enough to assess what fraction of patients has radiologically demonstrable hydrops from Meniere's disease or sudden deafness in general.

This study is also the first demonstration that the GE 3 T MR unit with 2D-FLAIR sequences could successfully detect the endolymphatic hydrops. The present findings confirm those of previous reports, in

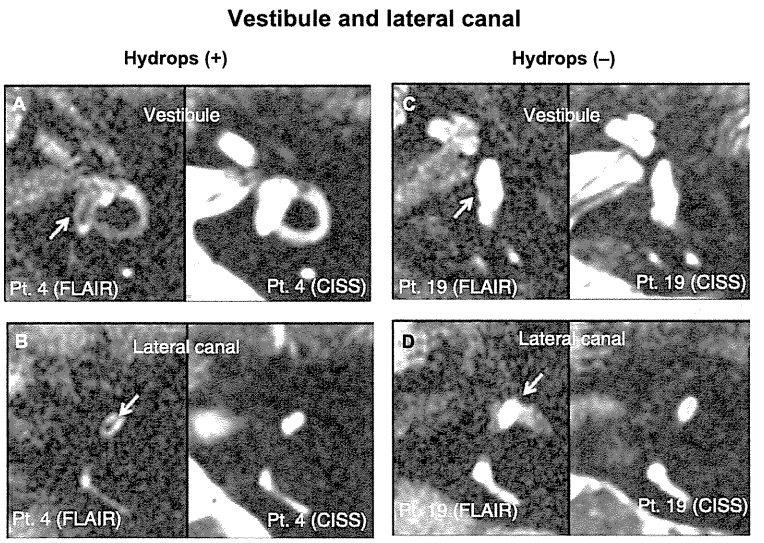

Figure 3. Hydrops-positive (A and B) and hydrops-negative (C and D) vestibule and lateral canal in 2D-FLAIR and CISS images. (A and B) In 2D-FLAIR images, enlarged vestibular (A) and lateral canal (B) endolymphatic space of vestibule was seen as low or no signal intensity area (arrows) surrounded by a gadolinium-enhanced high signal intensity perilymphatic space. (C and D) In 2D-FLAIR images, no remarkable low signal intensity area was found in the vestibule (C) and lateral canal (D). CISS images in the same plane were helpful in identifying inner ear structures. Numbers in the figures indicate patient ID numbers.

which Siemens 3 T MR units with 3D-FLAIR or 3D-real IR sequences were used and successfully visualized endolymphatic hydrops in patients with Meniere's disease [7–10], fluctuating hearing loss without vertigo [14], and delayed endolymphatic hydrops [15]. These results would be attractive, especially to researchers who have no access to a Siemens 3 T MR unit with 3D-FLAIR or 3D-real IR sequences, and may thus be hesitant to start a project on endolymphatic imaging.

In 1 of 10 patients with Meniere's disease (patient no. 1), gadolinium enhancement was very faint throughout the inner ear (data not shown), making it difficult to evaluate the images. This is probably because the permeability of gadolinium into the inner ear from the round window was poor. This finding is in line with that of Yoshioka et al., who reported that round window permeability was absent in 5% of patients with inner ear diseases [16]. In such a case, accurate evaluation of endolymphatic images was difficult. All the other nine patients with Meniere's disease had endolymphatic hydrops (Figure 4).

Regarding the endolymphatic image analysis on sudden deafness, Katayama et al. reported that none of four patients had endolymphatic hydrops as revealed by inner ear MRI with intratympanic gadolinium injection [17]. In the present study, two of eight patients with sudden deafness had endolympatic hydrops (patient nos 17 and 21). This is probably because inner ear MRIs in our study were taken several months after the onset of sudden deafness. It was not clear whether the hydrops in these patients existed from the early onset of sudden deafness or developed after the partial recovery from sudden deafness, because inner ear MRIs were not taken at the onset of sudden deafness. However, in any case, these hydrops were not causally related to the pathogenesis of sudden deafness of these patients. Therefore, it could be assumed that these may be cases of secondary hydrops after sudden deafness. If endolymphatic hydrops had been the primary cause of sudden deafness of these patients, the hydrops would have disappeared after partial recovery from hearing loss, which was not evident in these patients. Therefore, it was suggested that these were secondary hydrops cases. Temporal bone histologic studies have demonstrated that not only sudden deafness, but also other ear diseases, middle ear surgery, and temporal bone trauma, can cause secondary hydrops [18]. Thus, a clear distinction should be established between secondary hydrops and idiopathic endolymphatic hydrops, namely Meniere's disease. In the former cases, treatment for hydrops is nonsense and should be avoided even in the presence of hydrops in image analyses. It would be interesting to compare the rate of secondary hydrops between temporal bone histology and endolymphatic image analyses in future.

Table I. Patient profiles and location of endolymphatic hydrops.

Patient no.	Diagnosis	Sex	Age (years)	CP	EcochG	Hearing level (dB)	Interval (months)	Hydrops				
								Cochlea	Anterior canal	Lateral canal	Posterior canal	Vestibule
1	Left MD	M	28	Left 46%	+	53.75	84	Insufficient	Insufficient	Insufficient	Insufficient	Insufficient
4	Left MD	M	47	Left 26%	+	57.5	34	+*	–	+*	+	+*
5	Left MD	F	52	Left 66%	+	48.75	120	+	–	–	+	–
6	Left SD	F	38	Left 58%	–	110 (2K, 4K SO)	6	–*	–	–	–	–
8	Right MD	M	66	Right 54%	+	58.75	48	+*	–	+	+	+
14	Right MD	M	65	Right 30%	–	53.75	36	+	–	+	+	+
15	Left SD	M	46	NA	NA	54	6	–	–	–	–	–
17	Right SD	F	34	NA	–	58.75	11	+	+	–	+	+
19	Left SD	F	30	NA	NR	98.75 (2K, 4K SO)	1	–	–	–*	–*	–*
20	Right MD	F	46	Right 48%	+	51.25	48	+	+	+	+*	+
21	Left SD	F	64	Left 60%	NR	58.75	2	+	–	–	+	+
22	Right SD	F	26	NA	NA	92.5	7	–	–	–	–	–
23	Right MD	F	43	Right 66%	NR	63.75	154	+	+	–	+	+
24	Right SD	M	34	NA	NA	46.25	2	–	–	–	–	–
25	Right SD	M	52	Right 100%	NA	48.75	2	–	–	–	–	–
26	Right MD	F	45	Right 24%	–	51.25	180	+	+*	+	+	+
27	Right MD	M	43	Right 30%	+	52.5	48	+	+	+	+	+
29	Right MD	F	32	Right 68%	NR	0.5K, 1K, 2K, 4K SO	108	–*	–*	+	–	+

CP, canal paresis; EcochG, electrocochleogram (+, dominant -SP/AP-positive; –, dominant -SP/AP-negative); Hearing level, average of 500, 1000, 2000, and 4000 Hz; Insufficient, insufficient study due to low enhancement; Interval, interval between onset of disease and MRI examination; MD, Meniere's disease; NA, not applicable; NR, no response; SD, sudden deafness; SO, scale out.
*Figure is available.

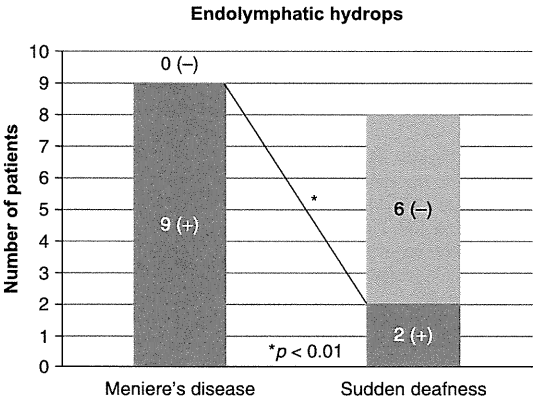

Figure 4. Number of hydrops-positive (+) and -negative (–) patients among patients with Meniere's disease and sudden deafness. Nine of the 10 patients with Meniere's disease had endolymphatic hydrops, whereas 2 of 8 patients with sudden deafness showed endolymphatic hydrops. *$p < 0.01$ by Fisher's exact test.

As shown in Figures 1–3 and Table I, it was possible to determine the exact location of endolymphatic hydrops in the inner ear. Endolymphatic hydrops in patients with Meniere's disease was most often observed in the cochlea, vestibule, and posterior canal, followed by the lateral and anterior canal (Table I). These results are roughly in accordance with histological findings in temporal bones from patients with Meniere's disease in which the frequency of endolymphatic hydrops was in the following decreasing order: cochlea, saccule, utricle, posterior canal, anterior canal, lateral canal [19]. These observations underscore the fact that the combination of inner ear MRI and intratympanic Gd injection can be used as a reliable tool for radiologic diagnosis of endolymphatic hydrops in patients with Meniere's disease.

Most patients with Meniere's disease (eight of nine) had hydrops in the cochlea (Table I), probably because only typical cases of Meniere's disease were investigated in this study. In future studies, it would be possible to correlate the location of endolymphatic hydrops and the type of disease, e.g. 'cochlear' type (fluctuating hearing loss without vertigo) or 'vestibular' type (recurrent vertigo without hearing loss) of Meniere's disease. Regarding the detection rate of cochlear hydrops, endolymphatic images were superior to EcochG (89% vs 60%), which corroborates the findings of a previous study [20]. In contrast, only 78% of patients with Meniere's disease with ipsilateral caloric weakness (CP% ≥ 24%) had endolymphatic hydrops in lateral canals. This is probably because canal paresis may not be a direct downstream event in endolymphatic hydrops, but the result of an indirect complex factor such as degeneration or dysfunction of hair cells.

Conclusion

The present study demonstrates that 2D-FLAIR sequences using a GE 3T MR unit can successfully detect endolymphatic hydrops when combined with intratympanic Gd injection. This is the first report showing that the detection rate of endolymphatic hydrops is significantly higher in patients with Meniere's disease than in those with sudden deafness, indicating that 3T MRI in combination with intratympanic Gd injection is a useful tool in the diagnosis of endolymphatic hydrops. However, secondary hydrops was also found in two of eight patients with sudden deafness, a condition that should be strictly distinguished from Meniere's disease in the diagnosis and treatment of inner ear diseases.

Acknowledgments

This study was partly supported by a research grant for intractable disease (vestibular disorder) from the Ministry for Health, Labor, and Welfare of Japan. The authors thank Dr Kalubi Bukasa for the critical reading of the manuscript. Results of this article were presented at the 45th Annual Spring Meeting for American Neurotology Society in Las Vegas, 26 th Barany Society Meeting in Reykjavik, and 6 th International Symposium on Meniere's Disease and Inner Ear Disorders in Kyoto.

Declaration of interest: The authors report no conflicts of interest. The authors alone are responsible for the content and writing of the paper.

References

[1] Committee on Hearing and Equilibrium. Committee on hearing and equilibrium guidelines for the diagnosis and evaluation of therapy in Meniere's disease. Otolaryngol Head Neck Surg 1995;113:181–5.

[2] Ito M, Watanabe Y, Shojaku H, Kobayashi H, Aso S, Mizukoshi K. Furosemide VOR test for the detection of endolymphatic hydrops. Acta Otolaryngol 1993;113:55–7.

[3] Salt AN, Henson MM, Gewalt SL, Keating AW, DeMott JE, Henson OW Jr. Detection and quantification of endolymphatic hydrops in the guinea pig cochlea by magnetic resonance microscopy. Hear Res 1995;88:79–86.

[4] Koizuka I, Seo Y, Murakami M, Seo R, Kato I. Micromagnetic resonance imaging of the inner ear in the guinea pig. NMR Biomed 1997;10:31–4.

[5] Zou J, Pyykkö I, Bretlau P, Klason T, Bjelke B. In vivo visualization of endolymphatic hydrops in guinea pigs: magnetic resonance imaging evaluation at 4.7 tesla. Ann Otol Rhinol Laryngol 2003;112:1059–65.

[6] Counter SA, Zou J, Bjelke B, Klason T. 3D MRI of the in vivo vestibulo-cochlea labyrinth during Gd-DTPA-BMA uptake. Neuroreport 2003;14:1707–12.

[7] Nakashima T, Naganawa S, Sugiura M, Teranishi M, Sone M, Hayashi H, et al. Visualization of endolymphatic hydrops in patients with Meniere's disease. Laryngoscope 2007;117:415–20.

[8] Naganawa S, Sugiura M, Kawamura M, Fukatsu H, Sone M, Nakashima T. Imaging of endolymphatic and perilymphatic fluid at 3T after intratympanic administration of gadolinium-diethylene-triamine pentaacetic acid. AJNR Am J Neuroradiol 2008;29:724–6.

[9] Naganawa S, Nakashima T. Cutting edge of inner ear MRI. Acta Otolaryngol Suppl 2009;560:15–21.

[10] Fukuoka H, Tsukada K, Miyagawa M, Oguchi T, Takumi Y, Sugiura M, et al. Semi-quantitative evaluation of endolymphatic hydrops by bilateral intratympanic gadolinium-based contrast agent (GBCA) administration with MRI for Meniere's disease. Acta Otolaryngol 2010;130:10–16.

[11] Nakashima T, Naganawa S, Pyykko I, Gibson WPR, Sone M, Nakata S, et al. Grading of endolymphatic hydrops using magnetic resonance imaging. Acta Otolaryngol 2009; 129:5–8.

[12] Kakigi A, Nishimura M, Takeda T, Okada T, Murata Y, Ogawa Y. Effects of gadolinium injected into the middle ear on the stria vascularis. Acta Otolaryngol 2008;128: 841–5.

[13] Yamasoba T, Kikuchi S, Sugasawa M, Yagi M, Harada T. Acute low-tone sensorineural hearing loss without vertigo. Arch Otolaryngol Head Neck Surg 1994;120:532–5.

[14] Teranishi M, Naganawa S, Katayama N, Sugiura M, Nakata S, Sone M, et al. Image evaluation of endolymphatic space in fluctuating hearing loss without vertigo. Eur Arch Otorhinolaryngol 2009;266:1871–7.

[15] Kasai S, Teranishi M, Katayama N, Sugiura M, Nakata S, Sone M, et al. Endolymphatic space imaging in patients with delayed endolymphatic hydrops. Acta Otolaryngol 2009;129: 1169–74.

[16] Yoshioka M, Naganawa S, Sone M, Nakata S, Teranishi M, Nakashima T. Individual differences in the permeability of the round window: evaluating the movement of intratympanic gadolinium into the inner ear. Otol Neurotol 2009;30: 645–8.

[17] Katayama N, Yamamoto M, Teranishi M, Naganawa S, Nakata S, Sone M, et al. Relationship between endolymphatic hydrops and vestibular-evoked myogenic potential. Acta Otolaryngol 2010;130:917–23.

[18] Merchant SN, Adams JC, Nadol JB Jr. Pathophysiology of Meniere's syndrome: are symptoms caused by endolymphatic hydrops? Otol Neurotol 2005;26:74–81.

[19] Okuno T, Sando I. Localization, frequency, and severity of endolymphatic hydrops and the pathology of the labyrinthine membrane in Menière's disease. Ann Otol Rhinol Laryngol 1987;96:438–45.

[20] Yamamoto M, Teranishi M, Naganawa S, Otake H, Sugiura M, Iwata T, et al. Relationship between the degree of endolymphatic hydrops and electrocochleography. Audiol Neurootol 2009;15:254–60.

Acta Oto-Laryngologica, 2011; 131: 951–957

informa
healthcare

ORIGINAL ARTICLE

Endolymphatic sac tumor with overexpression of V2 receptor mRNA and inner ear hydrops

TADASHI KITAHARA, CHIE MAEKAWA, KAORU KIZAWA, TAKEFUMI KAMAKURA, ARATA HORII & HIDENORI INOHARA

Department of Otolaryngology, Osaka University, School of Medicine, Osaka, Japan

Abstract

Conclusion: We reported previously that hyperactivation of vasopressin type-2 receptor (V2R)-mediated signaling in the endolymphatic sac could affect endolymphatic fluid metabolism, resulting in the pathogenesis of endolymphatic hydrops. Taken together with the present endolymphatic sac tumor (ELST) study, it is suggested that disorder of V2R signaling in the endolymphatic sac for any reason could be involved in the pathogenesis of endolymphatic hydrops. Although it is due to tumor genesis in ELST, it is idiopathic in nature in Meniere's disease. *Objective:* We encountered two cases of ELST showing Meniere's disease-like symptoms. Both cases were suspected of having endolymphatic hydrops using neuro-otological examinations. To clarify the histopathological diagnosis of ELST and the molecular pathogenesis of endolymphatic hydrops, we performed histopathological and molecular biological examinations of the endolymphatic sac. *Methods:* ELSTs in two rare cases were removed completely through the transmastoidal approach. V2R mRNA expression was examined using real-time PCR. *Results:* The first case was diagnosed as inflammatory granulation adjacent to the endolymphatic sac, i.e. pseudo-ELST, and the second case was diagnosed as papillary adenoma of ELST. V2R mRNA expression was up-regulated in the endolymphatic sac of both cases as seen in Meniere's disease compared with controls.

Keywords: *Endolymphatic hydrops, Meniere's disease*

Introduction

Endolymphatic sac tumors (ELSTs) are extremely rare tumors of the petrous temporal bone, comprising approximately 4% of temporal bone lesions [1]. The first reported case of a tumor arising from the endolymphatic sac was discovered during sac decompression for presumed unilateral Meniere's disease (MD) in 1984 [2]. Actually, patients with ELST demonstrate MD-like symptoms, i.e. episodic vertigo accompanied by unilateral hearing loss and tinnitus [3]. We experienced two cases of ELST with MD-like symptoms during 2004–2010. Furthermore, both cases were suspected of having inner ear hydrops by positive signs in the glycerol test (G-test) and electrocochleogram (ECoG), which are the most reliable neuro-otological examinations for inner ear hydrops [4]. During tumor removal surgery, we obtained endolymphatic sac tissues from the affected areas for two purposes: the histopathological diagnosis of ELST and investigation of the molecular pathogenesis of inner ear hydrops.

Based on our recent molecular biological studies of the endolymphatic sac in MD [5,6] and delayed endolymphatic hydrops [7], strong relationships were revealed between the pathogenesis of inner ear hydrops and the intracellular signal cascade of antidiuretic stress hormone vasopressin type-2 receptor (V2R) in the endolymphatic sac. Therefore, in the present ELST study, we focused on V2R expression in the endolymphatic sac. We describe the two cases of ELST mentioned above with molecular biological data of the endolymphatic sac and discuss the mechanisms of generation of inner ear hydrops.

Correspondence: Tadashi Kitahara MD PhD, Department of Otolaryngology, Osaka University, School of Medicine, 2-2 Yamada-oka, Suita-city, Osaka 565-0871, Japan. Tel: +81 6 6879 3951. Fax: +81 6 6879 3959. E-mail: tkitahara@ent.med.osaka-u.ac.jp

(Received 14 March 2011; accepted 3 April 2011)

ISSN 0001-6489 print/ISSN 1651-2251 online
DOI: 10.3109/00016489.2011.580004

Material and methods

The use of all the human materials in the present study was approved by the Ethics Committee of Osaka University, School of Medicine (certificate number: 0424).

Diagnosis and surgery

Between 2004 and 2010, we experienced two cases of ELST out of 787 patients with MD (0.25%: 2/787) at the Dizziness & Vertigo Section in the Department of Otolaryngology, Osaka University Hospital. MD is diagnosed according to the criteria of AAO-HNS (1995) [8]. Cases were clinically diagnosed by imaging examination and histopathologically diagnosed by histopathological examination.

Case 1

A 43-year-old female patient presented to our hospital in 2006 with complaints of episodic vertigo accompanied by hearing loss and tinnitus in the right ear. She had suffered from those symptoms since 2002. She showed left-sided moderate sensorineural hearing loss with positive signs in the G-test (Figure 1A) and ECoG, and left-sided severe semicircular canal paresis with right-directed spontaneous nystagmus at the

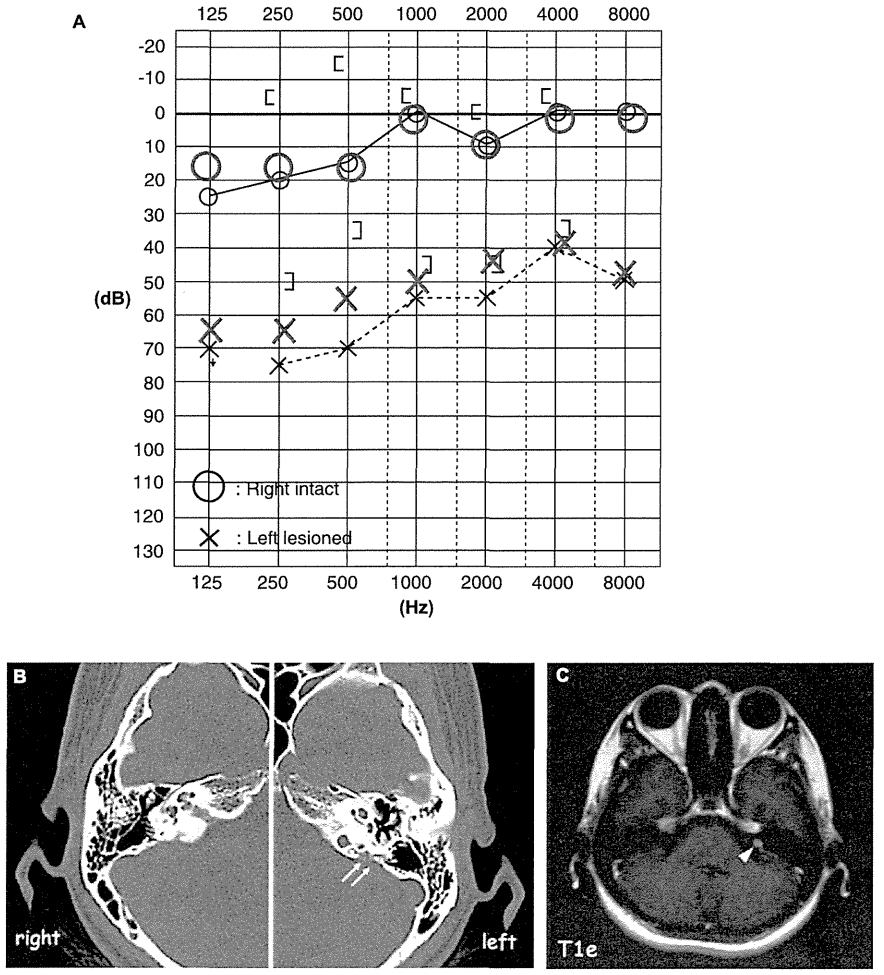

Figure 1. Audiogram (A), CT (B), and MRI (C) findings in case 1. (A) Case 1 showed left-sided moderate sensorineural hearing loss with positive glycerol test at the first visit, suggesting left Meniere's disease at that time. The gray-colored O and X stand for hearing level 2 h after 2.6 ml/kg of 50% glycerol intake in the right side and left side, respectively. (B) CT demonstrated bony erosion around the retrolabyrinthine air cells (arrows) in the left ear. (C) MRI revealed a T1-weighted gadolinium-enhanced lesion (T1e) at the area concerned with CT findings above (arrowhead), diagnosed as left endolymphatic sac tumor.